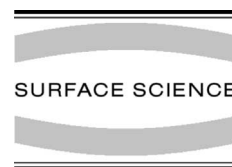




ELSEVIER

Surface Science 479 (2001) 69–82



www.elsevier.nl/locate/susc

# Thermal chemistry of toluene and benzene on Si(1 0 0) $2 \times 1$ and modified surfaces

Q. Li, K.T. Leung \*

*Department of Chemistry, University of Waterloo, Waterloo, Ont., Canada N2L 3G1*

Received 21 September 2000; accepted for publication 15 February 2001

## Abstract

The effects of methyl substitution on the room-temperature (RT) adsorption and reactivity of toluene on Si(1 0 0) $2 \times 1$  have been investigated by thermal desorption spectrometry (TDS), low energy electron diffraction (LEED), and Auger electron spectroscopy (AES). The similarities in the exposure dependence of the molecular desorption profiles of  $d_8$ -toluene and those of  $d_6$ -benzene suggest that both molecules have similar adsorption configurations on the  $(2 \times 1)$  surface. In particular, three molecular desorption features are found and can be attributed to adsorption on the single-dimer, double-dimer, and defect sites. However, the higher coverage and much lower molecular desorption of toluene than those of benzene suggest that the majority of adsorbed toluene has undergone other surface reactions during the TDS experiment. In addition to the weak molecular desorption, strong recombinative hydrogen desorption at 820 K, characteristic of hydrogen coming from mono-hydride (Si–H) surface species, is observed for toluene. The lack of a correspondingly strong  $D_2$  desorption peak for the RT exposure of  $d_6$ -benzene to Si(1 0 0) $2 \times 1$  indicates that the deposition of D atoms results from hydrogen abstraction from the methyl group of  $d_8$ -toluene. Since a RT post-exposure of atomic hydrogen to Si(1 0 0) $2 \times 1$  saturated with  $d_8$ -toluene does not appear to increase molecular desorption, the observed hydrogen abstraction therefore occurs upon adsorption and appears to be an irreversible process at RT. The difference in the  $D_2$  desorption profiles between toluene and  $D_2$  on Si(1 0 0) $2 \times 1$  suggests, in addition to hydrogen desorption, other surface processes including condensation polymerization and/or dissociative desorption that occur at 750–950 K. The Si(1 0 0) $2 \times 1$  surface is found to be more active in hydrogen abstraction and toluene dissociation than Si(1 1 1) $7 \times 7$ . For a RT exposure of  $d_8$ -toluene ( $d_6$ -benzene) to a sputtered Si(1 0 0) surface, the presence of an additional broad mass 4 desorption band at  $\sim 600$  K suggests the presence of a range of pathways by which  $D_2$  evolves directly from the dissociation of adsorbed  $d_8$ -toluene. A RT exposure of  $O_2$  to Si(1 0 0) $2 \times 1$  pre-adsorbed with  $d_8$ -toluene ( $d_6$ -benzene) is found to induce a substantial increase in the mass 4 desorption. The increase in the dissociation can be attributed to either surface-mediated oxidation or an  $O_2$ -induced process that stabilizes the adsorbed molecules to a higher temperature at which dehydrogenation and dissociation occur. © 2001 Elsevier Science B.V. All rights reserved.

**Keywords:** Thermal desorption spectroscopy; Auger electron spectroscopy; Chemisorption; Aromatics; Silicon; Low index single crystal surfaces; Solid–gas interfaces

\* Corresponding author. Tel.: +1-519-888-4567, ext.: 5826; fax: +1-519-746-0435.

E-mail address: tong@uwaterloo.ca (K.T. Leung).

## 1. Introduction

Organic semiconductors have attracted much recent attention because of their unique physical and electronic properties and of their potential applications in the microelectronic industry [1–4]. Many applications rely on the growth of organic thin films made from conducting polymers [5], which is an inherently disordered process due to the lack of control of the interfacial chemistry between the organic film and the supporting substrate. With its special structural and electronic properties [6,7], Si(100) has become one of the most important substrates for the microelectronics industry [8,9]. In recent years, studies of the interactions of unsaturated hydrocarbons with Si(100) have produced many promising opportunities for the development of atomically well-defined and ordered surface functionality [10–12]. Basic research on the surface chemistry of unsaturated cyclic hydrocarbons on silicon therefore helps to elucidate some of the important factors that govern the stability and selectivity of multifunctional organic films.

Benzene and toluene are two of the most important unsaturated cyclic hydrocarbons in organic chemistry. Since toluene differs from benzene chemically only with the replacement of a hydrogen atom by a methyl group, comparison of the surface chemistries of these aromatic compounds on the technologically important silicon surfaces may provide new insight into the formation of multifunctional organic films involving unsaturated cyclic hydrocarbons. Although the interaction of benzene with silicon has been widely studied by a variety of theoretical [13–15] and experimental techniques including thermal desorption spectrometry (TDS) [16,17], high resolution electron energy loss spectroscopy [17], photoemission [18,19], infrared spectroscopy and near-edge X-ray absorption fine structure [20], and scanning tunnelling microscopy (STM) [21–24], only a limited amount of work has been found for toluene [25,26]. Previous studies from our group have shown that the methyl group could have interesting effects on the adsorption and reactivity of aromatic compounds on pristine and modified surfaces of Si(111)7 × 7 [25,27]. More recently, Borovsky et al. reported a STM study on the ad-

sorption of toluene on Si(100)2 × 1 [26], which suggests that room temperature (RT) adsorption occurs only on top of the dimer rows, giving rise to several binding geometries that closely resemble those of benzene. The interactions of toluene and xylenes with Si(100) were also investigated using Fourier-transform infrared spectroscopy (FTIR) by Coulter et al. [28]. These FTIR spectra show that the methyl-substituted aromatic hydrocarbons are chemisorbed on Si(100) in much the same way as benzene, with some dissociation occurring upon adsorption, which likely arises from C–H bond cleavage of the substituent leaving the ring intact [28]. In the present work, we examine the interactions of toluene and benzene with the Si(100)2 × 1 and related surfaces using TDS, low energy electron diffraction (LEED) and Auger electron spectroscopy (AES), in order to compare the effects of methyl substitution between the (100) surface identified in the present work and the (111) surface observed in our earlier work [25,27]. Furthermore, the interactions of atomic hydrogen and O<sub>2</sub> with adsorbed toluene and benzene are also investigated. It is important to emphasize that theoretical analysis of the TDS profiles [29] along with examples from our early work [25,30,31] have shown the potential ambiguities in the interpretation of multiple desorption peaks in TDS experiments. In particular, individual desorption features in a TDS profile may be attributed either to separate adsorption states with different binding energies (corresponding to different adsorption geometries) or to a single adsorption state with a coverage-dependent adsorption energy [29]. Such ambiguities make it difficult to definitely identify the number and nature of the adsorption states and their relative populations from TDS data alone. Recent STM experiments can however alleviate some of these problems by identifying different adsorption features. In the present work, we take advantage of collaborating evidence provided by other studies.

## 2. Experimental

The experiments were conducted in a home-built double-chamber, ultra-high vacuum system with a

base pressure better than  $5 \times 10^{-11}$  Torr [27]. Briefly, the upper sample preparation chamber was used for ion sputtering, sample annealing and gas dosing, while the lower analysis chamber was equipped with a reverse-view four-grid retarding field analyser for LEED and AES analyses and with a 1–300 amu quadrupole mass spectrometer (QMS), differentially pumped in a separate housing, for TDS studies. The two chambers could be isolated from each other by a gate valve to minimize cross contamination during sample preparation involving reactive gases. The only entrance to the ionization region of the QMS was a 2 mm diameter orifice in the QMS chamber, which was found to be highly effective at reducing interference due to ambient desorption from the manipulator during a TDS experiment [27].

A  $12.5 \times 3.5$  mm<sup>2</sup> substrate was cut from a polished p-type boron doped Si(100) wafer (0.4 mm thick) with a resistivity of 0.0080–0.0095  $\Omega$  cm. The low resistivity of the sample allowed us to control the sample temperature smoothly by directly passing an appropriate current through the sample. The Si sample was mechanically fastened to a sample holder at both ends by Mo supporting plates and retaining bars, with small Si spacers sandwiched in between the Mo supports and the Si sample to minimize thermal contact between the sample and the rest of the manipulator while maintaining a good electrical connection. A type K thermocouple was inserted in between the Si spacers and mechanically fastened to one end of the Si sample by a Mo bar. In order to prevent any possible reaction between the Si sample and the thermocouple during annealing, the thermocouple was wrapped in a piece of Ta foil. Since the thermocouple was electrically in contact with the Si sample, an AC power supply was used to deliver the current in order to minimize any voltage difference across the finite thermocouple joint. A home-built programmable proportional–integral–differential temperature controller based on the TMS320c50 microprocessor [32] was used to provide linear temperature ramping at an adjustable heating rate, typically set at 1 K/s for the present TDS experiments. The standard deviation of the linear temperature ramping was better than  $\pm 1$  K and the temperature uniformity of the sample was

found to have at most 10% variation (at 1000 K). Given that the temperature was not uniform across the entire sample during annealing and that the temperature was not measured at the desorption point, the temperature difference between the sampling point of the thermocouple (edge of the sample) and the desorption point (centre of the sample) was determined and found empirically to be approximately proportional to the difference between the thermocouple sampling point and RT. The temperature at the desorption point was then calibrated according to standard TDS profiles for benzene and D<sub>2</sub> published in the literature [17,48].

Before introduction into the vacuum chamber, the Si sample was first pre-cleaned by using a typical RCA procedure [33] that involves soaking in a basic peroxide solution consisting of equal parts of H<sub>2</sub>O<sub>2</sub> (~30%) and NH<sub>4</sub>OH (~30%) in 5–20 parts of water. After the bake-out, the sample was out-gassed at 900 K for 20 h until the pressure recovered to  $2 \times 10^{-10}$  Torr range. The temperature of the sample was then rapidly increased to 1500 K while carefully keeping the vacuum below  $1 \times 10^{-9}$  Torr. This rapid-anneal method [34] has been found to be very effective in removing carbon contamination for the first experiment. Since toluene was found to easily decompose upon annealing [26], the resulting carbon could contaminate the bulk above 1400 K by diffusion [34,35], which would eventually lead to a hazy surface after several experiments. The haziness of the surface was thought to be caused by surface roughness of a  $\sim 100$  nm size scale as a result of SiC formation [34–36]. To prolong the repeated usage of the same sample, we first reduced the near-surface carbon concentration to below an acceptable limit as monitored by AES by repeated cycles of Argon sputtering at a glancing angle and low-temperature annealing (<850 K), before we applied the high-temperature anneal to 1500 K. The resulting surface cleanliness was confirmed by a sharp  $2 \times 1$  LEED pattern at RT, and with no detectable Auger features attributable to C, O and S. Through high-temperature annealing, the majority of the surface defects could be eliminated and the small amount of surface C (<1%) could be reduced by dissolving into the bulk while concomitantly increasing the C content of the near-surface region.

Despite the effectiveness of our present modified cleaning procedure, the appearance of a hazy surface was noticeable after 20–30 experiments and a new Si sample was usually required after 50 TDS experiments.

The chemicals (toluene (99.8% purity),  $d_8$ -toluene (98% D atom purity) and  $d_6$ -benzene (99.6% D atom purity)) used in this study were obtained commercially from BDH and Cambridge Isotope Laboratories and were degassed by repeated freeze–pump–thaw cycles prior to use. Sample dosing was performed by back-filling the sample preparation chamber to an appropriate pressure, as monitored by an uncalibrated ionization gauge, with a precision leak valve. All exposures (in units of Langmuir (1 L =  $10^{-6}$  Torr s)) were performed at RT unless stated otherwise.

### 3. Results and discussion

#### 3.1. RT adsorption at various exposures

The TDS profiles of the parent mass (mass 92) obtained as a function of RT exposure for toluene on Si(100) $2 \times 1$  are shown in Fig. 1a. In addition to the parent mass (mass 92), other fragments including mass 91 ( $C_6H_5CH_2^+$ ), mass 65 ( $C_5H_5^+$ ) and mass 51 ( $C_4H_3^+$ ) were also monitored during the TDS experiments. Since their corresponding peak intensity ratios were found to be in good accord with the respective ratios of the cracking pattern of toluene [37], the detected mass fragments could be attributed to dissociation of molecularly desorbed toluene in the ionizer of the QMS. These profiles therefore indicate that toluene desorbs from Si(100) $2 \times 1$  molecularly. For exposures less than 0.25 L, a single desorption peak at 530 K ( $\gamma$  state) is observed. With increasing exposure, a new desorption peak at 430 K ( $\beta$  state) emerges along with the higher temperature peak ( $\gamma$  state). The  $\gamma$  state appears to reach saturation at a lower exposure than the  $\beta$  state. Within the absolute accuracy of our temperature measurement ( $\pm 20$  K), the desorption maxima of these states remain essentially unchanged with increasing exposure, indicating first-order desorption kinetics [38]. At higher exposure ( $>4$  L), a third desorption state ( $\alpha$

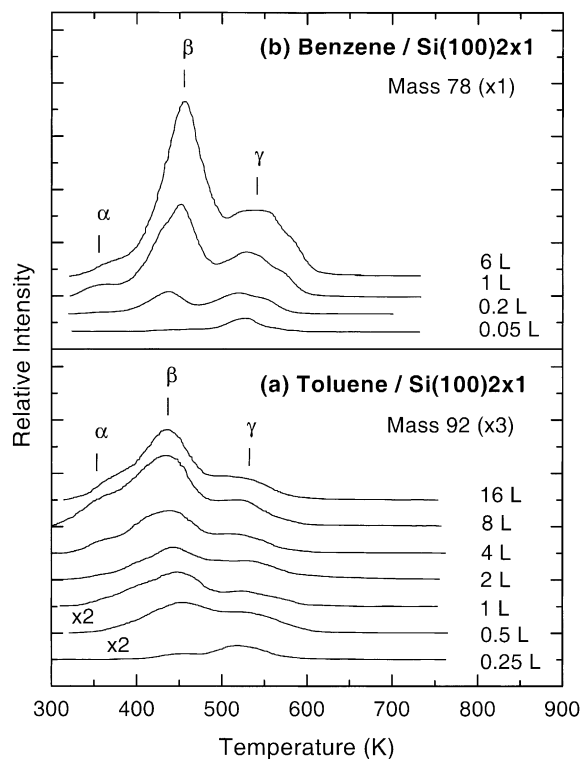


Fig. 1. Thermal desorption profiles of (a) mass 92 (molecular toluene) and (b) mass 78 (molecular benzene) as a function of RT exposure of toluene and benzene, respectively, to Si(100) $2 \times 1$ . The desorption intensity of toluene is found to be considerably smaller than that of benzene.

state) appears as a small shoulder at 350 K, which is much higher than the temperature generally expected for desorption from physisorbed aromatic molecules (e.g., the physisorption temperature for benzene is near 150 K [17]).

Fig. 1b gives the corresponding TDS profiles of the parent mass (mass 78) as a function of RT exposure for benzene on Si(100) $2 \times 1$ . Our data are found to be consistent with the earlier TDS results reported by Taguchi et al. [17]. Evidently, three desorption features are also observed. Except for the small differences in the desorption maxima from the corresponding TDS features for toluene (Fig. 1a), all three states also appear to follow first-order desorption kinetics. A number of studies, including several theoretical studies [13–15,19,24], have been made in an attempt to better understand the nature of the two more prominent features

( $\beta$  and  $\gamma$  states) of benzene on Si(100) $2 \times 1$ . In particular, two types of chemisorbed states were observed for the RT adsorption of benzene on Si(100) by using TDS [17] and STM [21,22]. Taguchi et al. attributed the two prominent TDS features for the  $\beta$  and  $\gamma$  states to benzene molecularly adsorbed on terrace and defect sites, respectively [17]. A recent study by Birkenheuer et al. suggested that a 1,4-cyclohexadiene-like “butterfly” structure di- $\sigma$  bonded to a dimer of the ( $2 \times 1$ ) surface (the so-called 1,4-single-dimer configuration) is energetically more favourable and should therefore be attributed to the lower-temperature desorption peak ( $\beta$  state) [15]. Another plausible bonding arrangement is a “tilted” 1,2-cyclohexadiene-like structure di- $\sigma$  bonded to a dimer of the surface (the 1,2-single-dimer configuration). In addition to these single-dimer geometries, various cyclohexene-like or cyclohexane-radical structures tetra- $\sigma$  bonded to two dimers of the ( $2 \times 1$ ) surface are possible. These double-dimer configurations give rise to the symmetric bridge, “tilted” tight bridge and twisted bridge geometries [21,22]. Lopinski et al. also suggested that the 1,4-single-dimer configuration responsible for the  $\beta$  state is metastable and converts to the double-dimer configuration ( $\gamma$  state) [21,22]. Using more refined calculations, the same group later associated the  $\beta$  state to the double-dimer “tight bridge” configuration that is converted from a metastable 1,4 single-dimer configuration, and the  $\gamma$  state to a double-dimer “C defect-twisted bridge” geometry [24].

As the molecular desorption features for both benzene and toluene on Si(100) $2 \times 1$  are found to have very similar desorption maxima and desorption kinetics, we hypothesize that RT adsorption of toluene involves similar bonding arrangements to those of benzene, with  $\beta$  and  $\gamma$  states involving, respectively, single-dimer and double-dimer bonding configurations (similar to those aforementioned for benzene) and the  $\alpha$  state related to defect sites. Indeed, the STM images of toluene on Si(100) at a low exposure ( $<0.1$  L) reported by Borovsky et al. [26] have revealed two features that closely resemble those observed for benzene on Si(100) [21–24], except that toluene appears to interact with more than two dimers on the ( $2 \times 1$ )

surface. Based on the physical dimensions of a toluene molecule (whereby the diameter of the aromatic ring is 2.8 Å and the C–C bond length between the ring and the methyl group is 1.5 Å) and given that the dimer separation and bond length between the dimer molecules are 3.8 and 2.3 Å respectively [39], the methyl group can be sufficiently close to an adjacent dimer atom only for toluene adsorption with the 3,4 configuration (denoting C atoms 3 and 4 with respect to the C atom 1 that bonds to the methyl group) on a single-dimer. In the case of the double-dimer configurations (and other single-dimer configurations), the methyl group is orientated away from the Si back bond and any unoccupied dangling bonds. The  $\beta$  state should therefore be more reactive than the  $\gamma$  state.

One significant difference between the adsorption of the two aromatic compounds on Si(100) $2 \times 1$  is that the desorption of toluene is considerably weaker than that of benzene for the same RT exposure. Assuming similar ionization cross-sections for benzene and toluene (consistent with their similar gas-phase cracking patterns observed by QMS), the amount of molecular desorption for toluene is approximately 10% of that for benzene. This greatly reduced desorption can be attributed to either a lower initial adsorption of toluene than benzene, or the presence of subsequent reactions that reduce the concentration of adsorbed toluene, or both. AES measurements were also employed to study toluene adsorption on Si(100) $2 \times 1$  at RT. Fig. 2 compares the relative carbon concentration, as indicated by the peak-to-peak ratio of the C(KLL) Auger peak relative to that of the Si(LVV) Auger peak, as a function of RT exposure for toluene and benzene on Si(100) $2 \times 1$ . For each exposure, the average value of three measurements is used to prevent the possible errors due to electron beam effects [40]. The ratio appears to reach its maximum value at 10 L exposure, which indicates completion of adsorption of the first monolayer (ML). This adsorption uptake curve is nearly identical to that represented by the total desorption intensity for the corresponding TDS measurements (not shown). The estimated saturation coverage of benzene has been determined to be 0.27 ML by

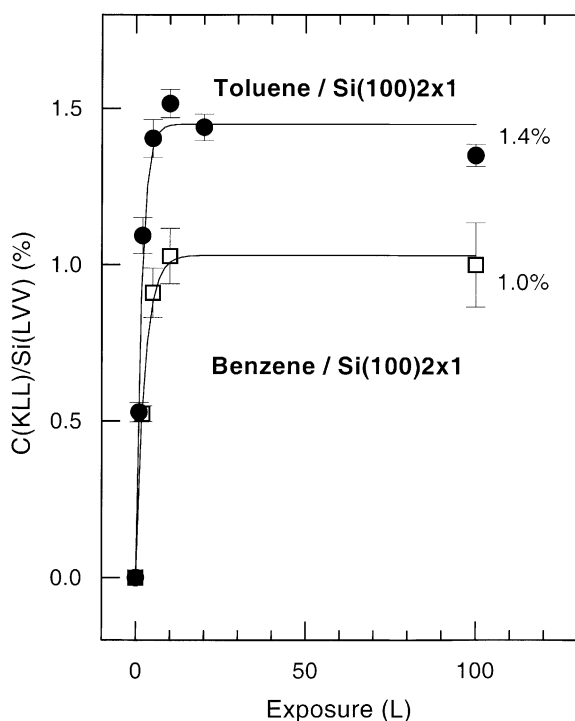


Fig. 2. Carbon moiety as reflected by the peak-to-peak intensity ratio for the C(KLL) to Si(LVV) Auger transitions as a function of RT exposure of toluene (●) and benzene (□) to Si(100)2 × 1. The Auger peak-to-peak ratios for toluene and benzene converge to 1.4% and 1.0%, respectively, at saturation coverage.

Taguchi et al. [17]. From the ratio of the saturation ratios of toluene (1.4%) and benzene (1.0%) and after taking the number of carbon atoms in toluene (7) and benzene (6) into account, we determine the saturation coverage for toluene to be 0.33 ML. The adsorption of toluene on Si(100)2 × 1 is therefore ~20% higher than that of benzene, which corresponds approximately to one toluene molecule for two pairs of Si dimers on the 2 × 1 surface. This result suggests that the weak molecular desorption observed for toluene is not due to lower coverage but rather to possible reactions that reduce the toluene concentration. In addition, the higher saturation coverage for toluene relative to benzene indicates a stronger adsorbate–substrate interaction than adsorbate–adsorbate interaction in the case of toluene on Si(100)2 × 1.

In an attempt to quantify such surface reactions during the annealing process, we monitored the carbon moiety for a saturation (100 L) exposure of toluene on Si(100)2 × 1 after annealing the sample to successively higher temperature. Fig. 3a shows that carbon depletion occurs in three stages involving different mechanisms. In accord with our TDS results (Fig. 1) that show weak molecular desorption of toluene in 320–600 K, only 10% reduction in the relative C moiety is observed from the AES results, therefore suggesting that only 10% of the adsorbed toluene undergoes molecular desorption. Between 750 and 950 K, a further 30% reduction in the carbon content is observed. Since our TDS experiments also reveal no significant molecular desorption in this temperature range, the considerable reduction in the C moiety can be attributed to thermal decomposition of toluene

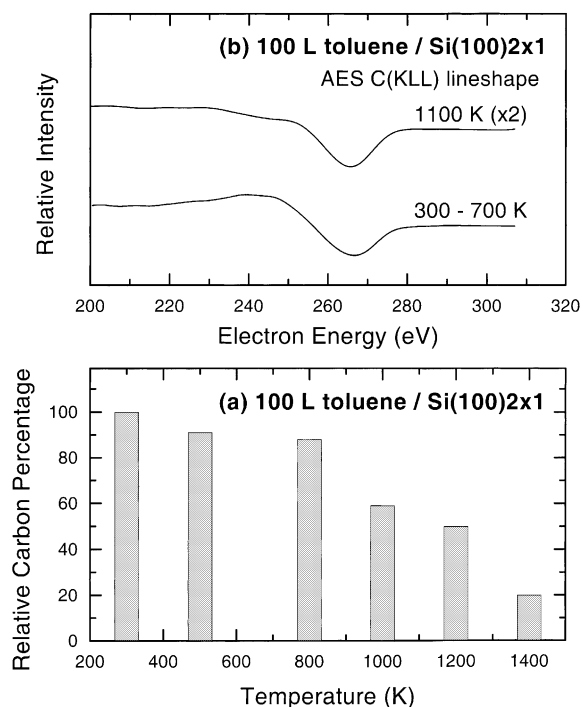


Fig. 3. (a) Relative carbon moiety change as a function of annealing temperature for a 100 L RT exposure of toluene on Si(100)2 × 1. (b) Typical line shapes for the corresponding derivative C(KVV) Auger transitions after annealing the sample in 300–700 K (lower curve) and to 1100 K (upper curve). The lower and upper curves are characteristic of the line shapes commonly found for SiC and graphites, respectively [43].

into hydrocarbon fragments that may undergo subsequent desorption in this temperature range. This could also be accompanied by associative hydrogen desorption with atomic hydrogen coming from the mono-hydride (Si–H) phase [41,42] (see Section 3.2 below). Finally, a significant carbon reduction occurs above 1200 K due to carbon diffusion into the bulk.

The above picture is supported by the changes in the line shape of the C(KLL) Auger peak for a 100 L RT exposure of toluene on Si(1 0 0) $2 \times 1$  upon annealing the sample to different temperatures. In particular, Fig. 3b shows that the Auger line shape changes from that characteristic of tetrahedrally ( $sp^3$ ) bonded C between RT and 700 K, to that representative of graphite ( $sp^2$  bonding) upon further annealing to 1100 K for 10 min [43]. The change in the Auger line shape is therefore consistent with the above hypothesis of thermal decomposition of adsorbed toluene in the 750–950 K range, likely resulting in the formation of carbon cluster or graphite-like islands through a possible condensation polymerization reaction of the toluene adsorbed on the surface. This type of condensation reaction is known to be assisted by the presence of homosystemic or heterosystemic hydrogen acceptors [44]. The Si(1 0 0) $2 \times 1$  surface with active dangling bonds along the dimer rows could serve as an ideal hydrogen acceptor.

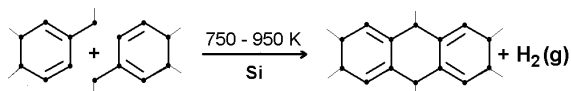


Fig. 4a shows a typical two-domain ( $2 \times 1$ ) LEED pattern of a clean Si(1 0 0) surface at RT collected at 71 eV electron energy. Upon exposure of 100 L of toluene to the clean surface at RT (Fig. 4a), the ( $2 \times 1$ ) LEED pattern remains essentially unchanged with a slight increase in the background intensity (Fig. 4b). It should be noted that, like benzene, a saturation coverage of toluene exhibits a two-domain ( $2 \times 1$ ) LEED pattern, and not a ( $2 \times 2$ ) or  $c(4 \times 2)$  LEED pattern as would be expected from a well-ordered overlayer (0.25 ML). Although benzene adsorption takes place in a regular fashion along the dimer rows of the domain by forming chains of benzene molecules bound to every other Si dimer, these chains are

very likely randomly registered relative to each other, resulting in an adsorption phase with one-dimensional disorder perpendicular to the Si(1 0 0) dimer rows, which slightly increases the background intensity [13]. Such a model proposed by Birkenheuer et al. [15] for benzene may be used to explain the similar LEED patterns observed for toluene adsorption, because there is no discernible difference observed in the LEED patterns for toluene or benzene adsorption on Si(1 0 0) $2 \times 1$ . Annealing a saturation coverage of toluene (0.33 ML) on the  $2 \times 1$  surface to 700 K does not appear to affect the ( $2 \times 1$ ) LEED pattern. However, further annealing the sample to 850 K for 5 min causes the LEED pattern to become diffuse (not shown), which indicates that the sample has undergone considerable reorganization. Adsorbates relocation, decomposition and other surface reactions contribute to binding of different fragments to the Si surface involving different bonding geometries, all of which can lead to a more diffuse LEED pattern. Further annealing the sample to 1100 K for 10 min recovers the basic two-domain ( $2 \times 1$ ) LEED pattern found for the clean surface but with additional streaks between the ( $2 \times 1$ ) spots, which can also be described as ( $2 \times n$ ) features (Fig. 4c). The  $2 \times n$  overlayer has been regarded as an intermediate structure between the ( $2 \times 1$ ) and  $c(4 \times 4)$  structures [45], and is likely due to carbon contamination [46,47]. The present LEED result is consistent with the STM results by Borovsky et al. [26], which also suggest that toluene decomposes upon annealing and the resulting dissociated hydrocarbon fragments form SiC and eventually coalesce to form graphite islands. The open areas not covered by those carbon islands would exhibit the normal ( $2 \times 1$ ) LEED pattern.

### 3.2. Hydrogen evolution

In addition to the weak molecular desorption features observed earlier (Fig. 1a), Fig. 5 shows considerably stronger mass 4 desorption at 820 K for a saturation exposure of deuterated toluene relative to that of deuterated benzene on Si(1 0 0) $2 \times 1$  at RT. It should be noted that the TDS profiles for normal and deuterated toluene are found to be identical, indicating no isotopic

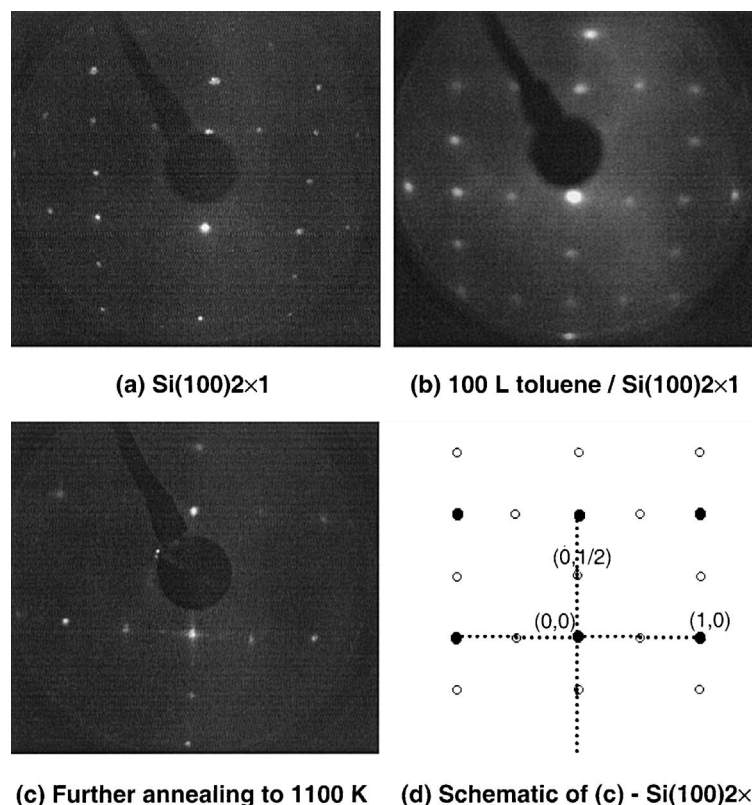


Fig. 4. LEED patterns collected at 71 eV electron beam energy for (a) clean Si(100) $2 \times 1$  at 300 K, (b) the Si(100) $2 \times 1$  surface exposed to 100 L of toluene at 300 K, followed by annealing to 700 K and (c) 1100 K for 10 min. (d) Schematic representation of the LEED pattern shown in (c).

effect on the adsorption process. Deuterated toluene is used in the present TDS experiment to avoid the large  $H_2$  background commonly found in stainless steel ultra-high vacuum chambers. The temperature of  $D_2$  evolution (820 K) is indicative of associative desorption of D atoms from monodeuteride (Si–D) on the silicon surface, rather than from the di-deuteride (Si– $D_2$ ) with a characteristic desorption maximum at 700 K [48]. Hydrogen evolution for  $d_8$ -toluene on Si(100) $2 \times 1$  may therefore involve partial dehydrogenation of adsorbed toluene to form Si–D and other fragments (e.g.,  $C_7$ -benzyl species [49]) and/or to complete dissociation of toluene into C and D atoms on the Si surface. In contrast to the small ratio of  $D_2$  evolution (mass 4) relative to molecular desorption (parent mass) for  $d_6$ -benzene (0.030), the corresponding ratio for  $d_8$ -toluene (15) is found to be

significantly larger, indicating that hydrogen evolution is a predominant pathway over molecular desorption for toluene. Given that the C–H bond strengths of  $C_6H_5-H$  and  $C_6H_5CH_2-H$  are typically 110 and 85 kcal/mol respectively [50], hydrogen evolution from the aromatic ring (aromatic hydrogen) for both benzene and toluene below the molecular desorption temperature (<600 K) therefore appears unlikely. Rather, the D atoms predominantly come from the methyl group (benzylic hydrogen) at this lower temperature. However, the prospect of minor hydrogen evolution pathways for benzene involving adsorption on defect sites cannot be ruled out [20]. Since a saturation coverage corresponds to one  $d_8$ -toluene molecule for every two Si dimers, only one out of the three possible benzylic D atoms can be sufficiently close to be abstracted by a neighbouring Si



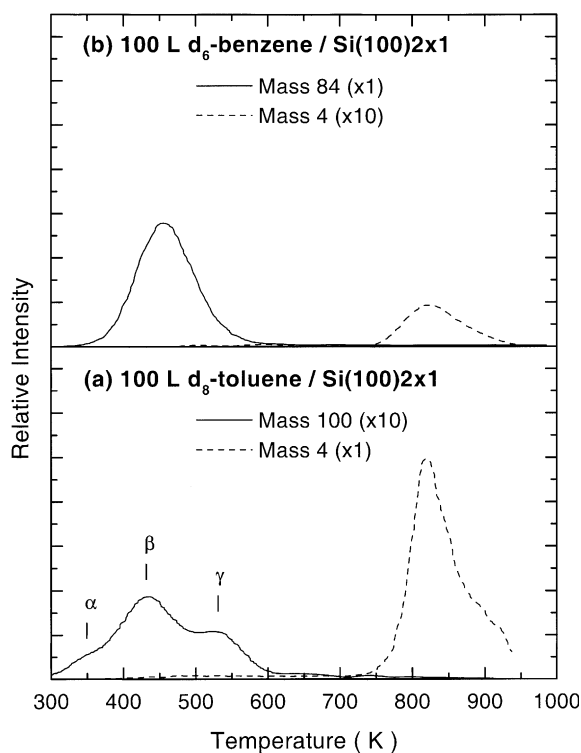


Fig. 5. Comparison of the molecular (—) and mass 4 (---) thermal desorption profiles of 100 L RT exposures of (a)  $d_8$ -toluene and (b)  $d_6$ -benzene to  $\text{Si}(100)2 \times 1$ . The parent masses for  $d_8$ -toluene and  $d_6$ -benzene correspond to mass 100 and mass 84, respectively.

dimer on the surface, which is consistent with the formation of Si–D structure. Finally, in order to determine whether hydrogen abstraction could occur upon adsorption of toluene, we saturated any unoccupied bonding sites with hydrogen atoms for a saturation coverage of  $d_8$ -toluene on  $\text{Si}(100)2 \times 1$  at RT. Dosing of atomic hydrogen was accomplished by exposing the sample with 2000 L of  $\text{H}_2$  with a hot W filament positioned 3 cm from the sample. Since blocking of the active sites by atomic hydrogen would prevent hydrogen abstraction (from the methyl group) to take place during the subsequent thermal annealing process, the lack of any increase in the molecular desorption features suggests that hydrogen abstraction has already occurred upon adsorption of toluene at RT. The abundance of hydrogen atoms on the surface after the post-exposure also does not ap-

pear to reverse the benzylic hydrogen abstraction of the methyl group in toluene, suggesting it to be an irreversible process at RT. The recent FTIR study by Coulter et al. also confirms that the dissociation of substituted aromatic molecules upon adsorption arises almost entirely by C–H bond cleavage of the functional group external to the aromatic ring [28].

The molecular desorption intensity for the  $\beta$  state relative to that for the  $\gamma$  state for  $d_8$ -toluene adsorption on  $\text{Si}(100)2 \times 1$  (Fig. 5a) is found to be considerably smaller than that for  $d_6$ -benzene adsorption (Fig. 5b – See also Fig. 1b). Since the adsorption of the benzene ring is expected to involve similar adsorption geometries, the presence of the methyl group in toluene evidently only affects the  $\beta$  state, which is consistent with the bonding model that the  $\beta$  state involves single-dimer configurations that are more susceptible to steric effects acting on the methyl group. On the other hand, the  $\gamma$  state involves the double-dimer configurations, whereby the methyl group is orientated away from the dimer and hence should have little effect on the adsorption.

Hydrogen evolution involving the Si–D bonding structure should follow the first-order desorption kinetics [41,42,51,52]. In contrast to a typical first-order desorption peak shape (i.e., with a faster drop-off at the higher temperature side), the slower drop-off at the higher temperature side of the mass 4 TDS peak observed in Fig. 5a indicates additional processes that increase hydrogen evolution at the higher temperature. According to our AES results that show increased depletion of carbon moiety in this temperature range (Fig. 3), we expect desorption of hydrocarbon fragments as a result of dissociation of adsorbed toluene. Associative desorption of D atoms also frees up more active sites on the surface, further enhancing hydrogen abstraction from the dissociated hydrocarbon fragments.

### 3.3. Effects of surface condition on thermal chemistry

Fig. 6 compares the TDS profiles of the parent mass (mass 100) and mass 4 for 100 L RT exposure

of  $d_8$ -toluene on the  $2 \times 1$  and amorphous Si(1 0 0) surfaces. An amorphous Si surface was produced by ion sputtering in  $2 \times 10^{-5}$  Torr of Argon for 1 h at 1 keV beam energy, and the lack of any long-range order was confirmed by the absence of a LEED pattern. The total areas for mass 100 and mass 4 for the amorphous surface (Fig. 6b) have been reduced by 1/3 and 3/5, respectively, relative to the  $2 \times 1$  surface (Fig. 6a). The general decrease in the overall intensity for the parent mass indicates reduction in the number of active sites available for molecular adsorption after Ar sput-

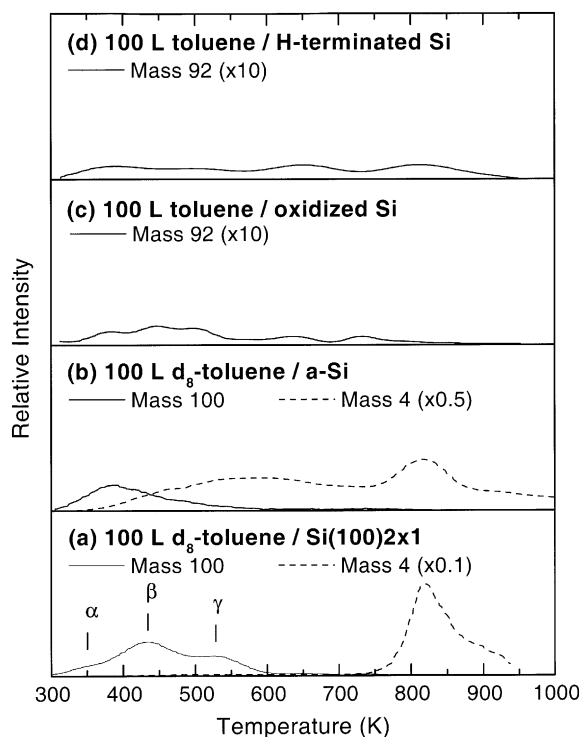


Fig. 6. Comparison of the molecular and mass 4 thermal desorption profiles for a 100 L RT exposure of ( $d_8$ -)toluene to the (a)  $2 \times 1$ , (b) amorphous, (c) oxidized, and (d) H-terminated surfaces of Si(1 0 0). An amorphous Si surface is obtained by ion sputtering in  $2 \times 10^{-5}$  Torr of Argon for 1 h at 1 keV beam energy. An oxidized Si surface is produced by exposing a clean  $2 \times 1$  surface with a 300 L exposure of  $O_2$  while a H-terminated Si(1 0 0) is prepared by exposing 2000 L of  $H_2$  to a clean  $2 \times 1$  surface with a hot W filament positioned 5 cm away. The parent masses for  $d_8$ -toluene (a,b) and normal toluene (c,d) correspond to mass 100 and mass 92, respectively.

tering. The weakening of peaks at 430 K ( $\beta$  state) and 530 K ( $\gamma$  state) for the amorphous Si surface is consistent with the general assignment of these states to terrace sites, while the strengthening of the TDS feature near 350 K clearly indicates that the  $\alpha$  state involves adsorption on defect sites. In Section 3.1, we propose that the  $\beta$  state involves adsorption in the single-dimer configurations, while the  $\gamma$  state involves the double-dimer bonding geometries. Furthermore, the presence of a broad new desorption band centered at 600 K in the mass 4 TDS profile indicates that hydrogen evolution originates from a variety of bonding geometries (all with its own adsorption energies). The source of the hydrogen atoms can be the absorbed toluene itself or any fragments resulting from thermal decomposition during the TDS experiment. Hydrogen abstraction from the methyl group opens up new opportunity for  $\sigma$ -bonding of the methylene group to the Si surface, which could provide the possibility for further reactions. In the case of  $d_6$ -benzene on sputtered Si [31], there is an increase in hydrogen evolution at  $\sim 800$  K, without any broad TDS feature near 600 K, indicating that the majority of benzene molecules has already desorbed molecularly before reaching this temperature.

The TDS profiles for a saturation coverage of normal toluene on an oxidized and H-terminated Si(100) are also shown in Fig. 6. An oxidized Si surface was obtained by exposing a clean Si(1 0 0) $2 \times 1$  with 300 L of  $O_2$  while a H-terminated Si(1 0 0) was prepared by exposing 2000 L of  $H_2$  to the  $2 \times 1$  sample with a hot W filament positioned 5 cm away. The TDS profiles for the parent mass are found to be featureless and greatly reduced in intensity after exposure of  $O_2$  or atomic H, suggesting that pre-exposure of oxygen and hydrogen has the effect of filling the active sites and hence preventing subsequent adsorption of toluene on Si(1 0 0) $2 \times 1$ .

### 3.4. Surface-mediated oxidation reaction

As shown in Fig. 7a, a 300 L  $O_2$  post-exposure to Si(1 0 0) $2 \times 1$  saturated with 100 L of  $d_8$ -toluene at RT is found to have a dramatic effect on the

TDS profiles of mass 100 (molecular desorption) and mass 4 ( $D_2$  evolution). The post-oxidation appears to greatly reduce molecular desorption of toluene while enhancing hydrogen evolution. In particular, the ratio of the integrated area for the mass 100 TDS profile to that of the mass 4 TDS profile is found to decrease from 0.07 to 0.01 by the  $O_2$  post-exposure. It therefore appears that post-oxidation greatly enhances the complete dissociation of  $d_8$ -toluene into C and D atoms on the Si surface. Fig. 7b shows similar effects for a 300 L post-exposure of  $O_2$  on  $Si(100)2 \times 1$  saturated with 100 L of  $d_6$ -benzene, whereby the ratio of the integrated area for the mass 84 TDS profile to that of the mass 4 TDS profile is found to reduce from 30 to 2 by the post-oxidation. Evidently, the enhanced dissociation of adsorbed toluene caused by post-oxidation is not exclusively

related to oxygen interaction with the methyl group, because post-oxidation also appears to facilitate dissociation of both toluene and benzene on  $Si(100)2 \times 1$ . It should be noted that neither benzene nor toluene readily reacts with  $O_2$  (g) in the absence of a catalyst [53,54]. The low temperature at which toluene (benzene) begins to desorb ( $\sim 350$  K) would suggest that either O reacts with the adsorbed toluene (benzene) directly near RT in a surface-mediated type reaction, or O stabilizes the adsorption of toluene (without a direct reaction) to a higher temperature at which hydrogen evolution occurs. The complete disappearance of the  $2 \times 1$  LEED pattern after  $O_2$  post-exposure is in favour of the former mechanism. The co-adsorption with  $O_2$  has also been found to increase the adsorption energy of  $NH_3$  on a Cu surface, resulting in the N–H bond breakage and the subsequent formation of hydroxyl species or  $H_2O$  [55].

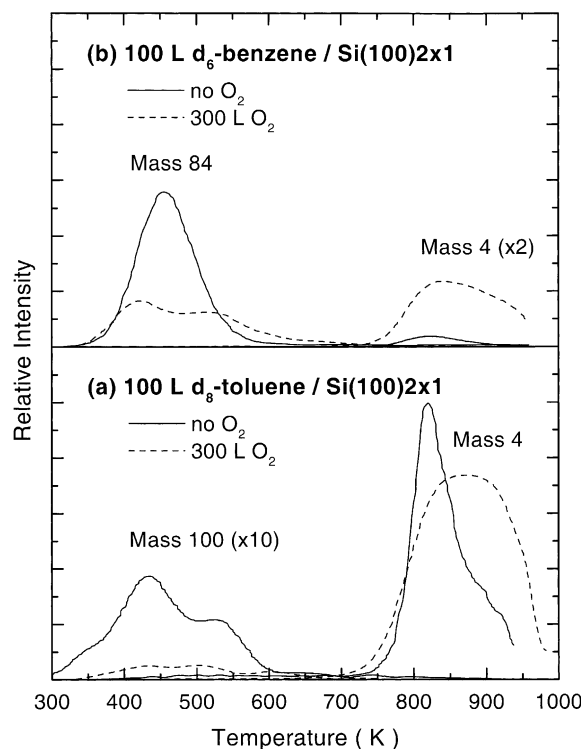
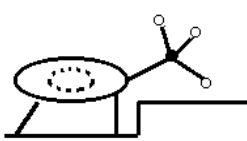
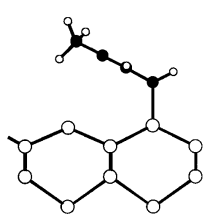
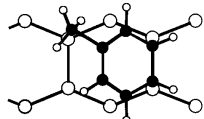
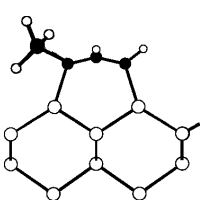
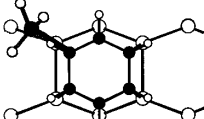
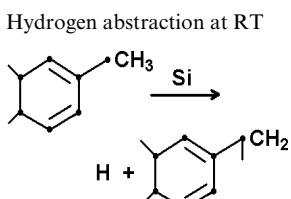
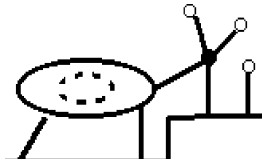
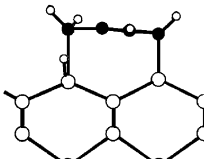
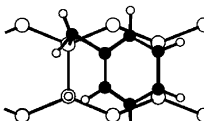
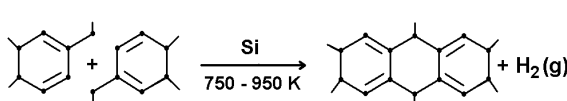
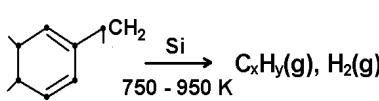


Fig. 7. Comparison of the molecular and mass 4 thermal desorption profiles of 100 L RT exposures of (a)  $d_8$ -toluene and (b)  $d_6$ -benzene to  $Si(100)2 \times 1$  with (---) and without (—) 300 L of  $O_2$  post-exposure. The parent masses for  $d_8$ -toluene and  $d_6$ -benzene correspond to mass 100 and mass 84, respectively.

#### 4. Concluding remarks

RT adsorption of toluene on the  $2 \times 1$  and modified  $Si(100)$  surfaces has been investigated by using TDS, AES and LEED, and the results are compared to that of benzene. Table 1 illustrates the key observations for toluene adsorption obtained in the present work. In particular, three molecular desorption states are observed at 350 K ( $\alpha$ ), 430 K ( $\beta$ ) and 530 K ( $\gamma$ ), which involve RT adsorption on defect sites, single-dimer and double-dimer geometries of  $Si(100)$ , respectively. The TDS data for toluene on sputtered Si surface confirms that the desorption peak at 350 K is related to adsorption on defect sites. Toluene in the double-dimer adsorption configuration ( $\gamma$  state) undergoes molecular desorption, while those in the  $\alpha$  and  $\beta$  states involve the loss of benzylic hydrogen at RT, leaving the methylene group bound to a neighbouring dimer on the surface. This result also favours the transformation from the  $\gamma$  state to the  $\beta$  state, and the resulting higher saturation coverage (0.33 M) for toluene than benzene (0.27 M) is supported by our AES results. Such hydrogen abstraction appears to stabilize the adsorbate on  $Si(100)$  at higher temperature and facilitate further reactions, such as condensation

Table 1  
Summary of plausible surface processes of toluene on Si(100)2 × 1 in various temperature ranges

Molecular desorption	$\alpha$ state 350 K	$\beta$ state 430 K	$\gamma$ state 530 K	
Adsorption configuration	 Defect site	 Side  Top Single-dimer	 Side  Top Double-dimer	
Hydrogen abstraction at RT			 Side  Top	N/A
Condensation polymerization				N/A
Dissociative desorption				N/A
Carbon diffusion into the Si bulk	1200–1400 K			N/A

polymerization and/or dissociation at 750–950 K. Further annealing to above 1200 K causes carbon diffusion into the bulk. In the case of benzene, three molecular desorption peaks are also ob-

served and found to have similar desorption maxima to those of the corresponding peaks for toluene. These TDS data therefore reflect the similarity in the nature of the adsorption states of

these aromatic molecules on Si(1 0 0) $2 \times 1$ . However, almost all of the adsorbed benzene undergoes molecular desorption without any evidence of further reactions at higher temperature. These differences show that toluene is more reactive than benzene toward the Si(1 0 0) surfaces. Surface roughness and post-oxidation also significantly improve the reactivity of aromatic compounds on Si surface.

In our previous TDS study of  $d_8$ -toluene on Si(1 1 1) $7 \times 7$  [25], two intense well-defined desorption peaks for the parent mass were observed at 370 and 420 K, which appear to have similar exposure dependence as the  $\beta$  and  $\gamma$  states for the Si(1 0 0) $2 \times 1$  surface observed in the present work. A weak mass 4 desorption at 800 K involving the Si–D configuration was also observed for the exposure of  $d_8$ -toluene to the  $7 \times 7$  surface. A broad mass 4 desorption peak at 540 K was observed for sputtered Si(1 1 1) surface and can be attributed to direct evolution of  $D_2$  during thermal dissociation of the adsorbed toluene. The presence of the mass 4 desorption peak at 800 K for the exposure of other selected deuterated isotopes ( $CH_3-C_6D_5$  and  $CD_3-C_6H_5$ ) and the lack of mass 4 evolution for the  $d_6$ -benzene exposure to Si(1 1 1) $7 \times 7$  suggest that deposition of D atoms on Si(1 1 1) is due to a methyl-to-surface interaction, which results in complete dissociation of the deuterated toluene samples. As with the Si(1 0 0) $2 \times 1$  surface, dissociation of toluene is found to be dramatically increased by a 2000 L  $O_2$  post-exposure on Si(1 1 1) $7 \times 7$ . The present study therefore shows that the general molecular desorption behaviour of toluene on Si(1 0 0) $2 \times 1$  is similar to that on Si(1 1 1) $7 \times 7$  [25], with minor differences in the temperatures for various desorption maxima. The significant differences in the extent for molecular desorption and hydrogen evolution show that Si(1 0 0) is more reactive than Si(1 1 1).

In summary, the present work shows the intricate thermal chemistry of toluene on Si(1 0 0). On the one hand, upon adsorption on such a well-ordered surface as Si(1 0 0) $2 \times 1$ , the aromatic ring of these cyclic hydrocarbon compounds exerts significant selectivity on the bonding configurations, and bonding through specific functional groups (such as the methyl group) might be en-

hanced by annealing [8]. On the other hand, the methyl group plays a decisive role in the subsequent thermal surface reactions, such as decomposition and condensation polymerization. Additional studies involving other techniques will be of great interest in providing further insights into the surface chemistry of aromatic hydrocarbons on Si(1 0 0).

## Acknowledgements

This work was supported by the Natural Sciences and Engineering Research Council of Canada.

## References

- [1] A. Tsumura, H. Koezuka, T. Ando, *Appl. Phys. Lett.* 49 (1986) 1210.
- [2] A. Garito, R.F. Shi, M. Wu, *Physics Today* 47 (1994) 51.
- [3] J.R. Ostrick, A. Dodabalapur, L. Torsi, A.J. Lovinger, E.W. Kwock, T.M. Miller, M. Galvin, M. Berggren, H.E. Katz, *J. Appl. Phys.* 81 (1997) 6804.
- [4] V.I. Krinichnuyi, *Phys. Solid State* 39 (1997) 1.
- [5] T.A. Skotheim, R.L. Elsenbaumer, J.R. Reynolds, *Handbook of Conducting Polymers*, Marcel Dekker, New York, 1998.
- [6] H.N. Waltenburg, J.T. Yates, *Chem. Rev.* 95 (1995) 1589.
- [7] R.J. Hamers, Y. Wang, *Chem. Rev.* 96 (1996) 1261.
- [8] R.J. Hamers, J.S. Hovis, C.M. Greenlief, D.F. Padowitz, *Jpn. J. Appl. Phys.* 38 (1999) 3879.
- [9] J.T. Yates Jr., *Science* 279 (1998) 335.
- [10] J.S. Hovis, R.J. Hamers, *J. Phys. Chem. B* 101 (1997) 9581.
- [11] M.D. Ellison, R.J. Hamers, *J. Phys. Chem. B* 103 (1999) 6243.
- [12] T. Bitzer, N.V. Richardson, *Appl. Phys. Lett.* 71 (1997) 662.
- [13] B.I. Craig, *Surf. Sci. Lett.* 280 (1993) L279.
- [14] H.D. Jeong, S. Ryu, Y.S. Lee, S. Kim, *Surf. Sci.* 344 (1995) L1226.
- [15] U. Birkenheuer, U. Gutdeutsch, N. Rosch, *Surf. Sci.* 409 (1998) 213.
- [16] C.D. MacPherson, D.Q. Hu, K.T. Leung, *Solid State Commun.* 80 (1991) 217.
- [17] Y. Taguchi, M. Fujisawa, T. Takaoka, T. Okada, M. Nishijima, *J. Chem. Phys.* 95 (1991) 6870.
- [18] Y. Taguchi, Y. Ohta, T. Katsumi, K. Ichikawa, O. Aita, *J. Electron. Spectrosc. Rel. Phenom.* 88–91 (1998) 671.
- [19] S. Gokhale, P. Trischberger, D. Menzel, W. Widdra, H. Droge, H.-P. Steinruck, U. Birkenheuer, U. Gutdeutsch, N. Rosch, *J. Chem. Phys.* 108 (1998) 5554.

- [20] M.J. Kong, A.V. Teplyakov, J.G. Lyubovitsky, S.F. Bent, *Surf. Sci.* 411 (1998) 286.
- [21] G.P. Lopinski, D.J. Moffatt, R.A. Wolkow, *Chem. Phys. Lett.* 282 (1998) 305.
- [22] G.P. Lopinski, T.M. Fortier, D.J. Moffatt, R.A. Wolkow, *J. Vac. Sci. Technol. A* 16 (1998) 1037.
- [23] B. Borovsky, M. Krueger, E. Ganz, *Phys. Rev. B* 57 (1998) R4269.
- [24] R.A. Wolkow, G.P. Lopinski, D.J. Moffatt, *Surf. Sci.* 416 (1998) L1107.
- [25] C.D. MacPherson, K.T. Leung, *Surf. Sci.* 326 (1995) 141.
- [26] B. Borovsky, M. Krueger, E. Ganz, *J. Vac. Sci. Technol. B* 17 (1999) 7.
- [27] C.D. MacPherson, D.Q. Hu, K.T. Leung, *Surf. Sci.* 322 (1995) 58.
- [28] S.K. Coulter, J.S. Hovis, M.D. Ellison, R.J. Hamers, *J. Vac. Sci. Technol. A* 18 (2000) 1965.
- [29] H. Froitzheim, P. Schenk, G. Wedler, *J. Vac. Sci. Technol. A* 11 (1993) 345.
- [30] C.D. MacPherson, D.Q. Hu, K.T. Leung, *Surf. Sci.* 276 (1992) 156.
- [31] C.D. MacPherson, K.T. Leung, *Surf. Sci.* 324 (1995) 202.
- [32] Texas Instruments TMS320C5X DSP Starter Kit User's Guide, Microprocessor Development Systems, Texas Instruments Inc., USA, 1994.
- [33] W. Kern, D.A. Puotinen, *RCA Rev.* 31 (1970) 187.
- [34] B.S. Swartzentruber, Y.-W. Mo, M.B. Webb, M.G. Lagally, *J. Vac. Sci. Technol. A* 7 (1989) 2901.
- [35] S.M. Lee, S.H. Lee, M.M. Sung, D. Marton, S.S. Perry, J.W. Rabalais, *IEEE Proc.*, 11th Int. Conf. Ion Implant Technol., 1997, p. 650.
- [36] A.W. Munz, Ch. Ziegler, W. Gopel, *Surf. Sci.* 325 (1995) 177.
- [37] NIST/EPA/NIH Mass Spectral Library, NIST'98 with windows, Version 1.7 software, 1996.
- [38] P.A. Redhead, *Vacuum* 12 (1962) 203.
- [39] J.A. Kubby, J.J. Boland, *Surf. Sci. Rep.* 26 (1996) 61.
- [40] C.C. Cheng, R.M. Wallace, P.A. Taylor, W.J. Choyke, J.T. Yates Jr., *J. Appl. Phys.* 67 (1990) 3693.
- [41] K. Sinniah, M.G. Sherman, L.B. Lewis, W.H. Weinberg, J.T. Yates Jr., K.C. Janda, *Phys. Rev. Lett.* 62 (1989) 567.
- [42] K. Sinniah, M.G. Sherman, L.B. Lewis, W.H. Weinberg, J.T. Yates Jr., K.C. Janda, *J. Chem. Phys.* 92 (1990) 5700.
- [43] A.K. Green, V. Rehn, *J. Vac. Sci. Technol. A* 1 (1983) 1877 and references therein.
- [44] J.R. Anderson, Q.-N. Dong, Y.-F. Chang, R.J. Western, *J. Catal.* 127 (1991) 113.
- [45] D.-S. Lin, P.-H. Wu, *Surf. Sci.* 397 (1998) L273.
- [46] K. Miki, K. Sakamoto, T. Sakamoto, *Appl. Phys. Lett.* 71 (1997) 3266.
- [47] H. Norenberg, G.A.D. Briggs, *Surf. Sci.* 430 (1999) 154.
- [48] M. Suemitsu, H. Nakazawa, N. Miyamoto, *Appl. Surf. Sci.* 82/83 (1994) 449.
- [49] N.R. Avery, *J. Chem. Soc. Chem. Commun.* 3 (1988) 153.
- [50] R.C. Weast (Ed.), *CRC Handbook of Chemistry and Physics*, 64th ed., CRC Press Inc., Boca Raton, 1983.
- [51] U. Hofer, L. Li, T.F. Heinz, *Phys. Rev. B* 45 (1992) 9485.
- [52] L.A. Okada, M.L. Wise, S.M. George, *Appl. Surf. Sci.* 82/83 (1994) 410.
- [53] R.A. Sheldon, N. de Heij, in: W. Ando, Y. Moro-Oka (Eds.), *The Role of Oxygen in Chemistry and Biochemistry*, Elsevier, Amsterdam, 1988, p. 243.
- [54] R.N. Patel, in: R.L. Augustine (Ed.), *Catalysis of Organic Reactions*, Marcel Dekker, New York, 1985, p. 327.
- [55] G.J.C.S. van de Kerkhof, W. Biemolt, A.P.J. Jansen, R.A. van Santen, *Surf. Sci.* 284 (1993) 361 and references therein.